Supplementary materials

Electrolyte-affinitive porous separators enabled by nitrile integration and polymerization-induced phase separation for stable lithium metal batteries

Hori Kim, Jae Yul Ryu, Minsung Kim, Hyuk-Joon Kim, Youngsin Kim and Joon Hak Oh*

H. Kim, J. Y. Ryu, M. Kim, Prof. J. H. Oh

School of Chemical and Biological Engineering, Institute of Chemical Processes, Seoul National University, 1 Gwanak-ro, Gwanak-gu, Seoul 08826, Republic of Korea

E-mail: joonhoh@snu.ac.kr

H.-J. Kim, Y. Kim
Department of Materials Science and Engineering, Research Institute of Advanced Materials (RIAM), Seoul National University, 1 Gwanak-ro, Gwanak-gu, Seoul 151-742, Republic of Korea.

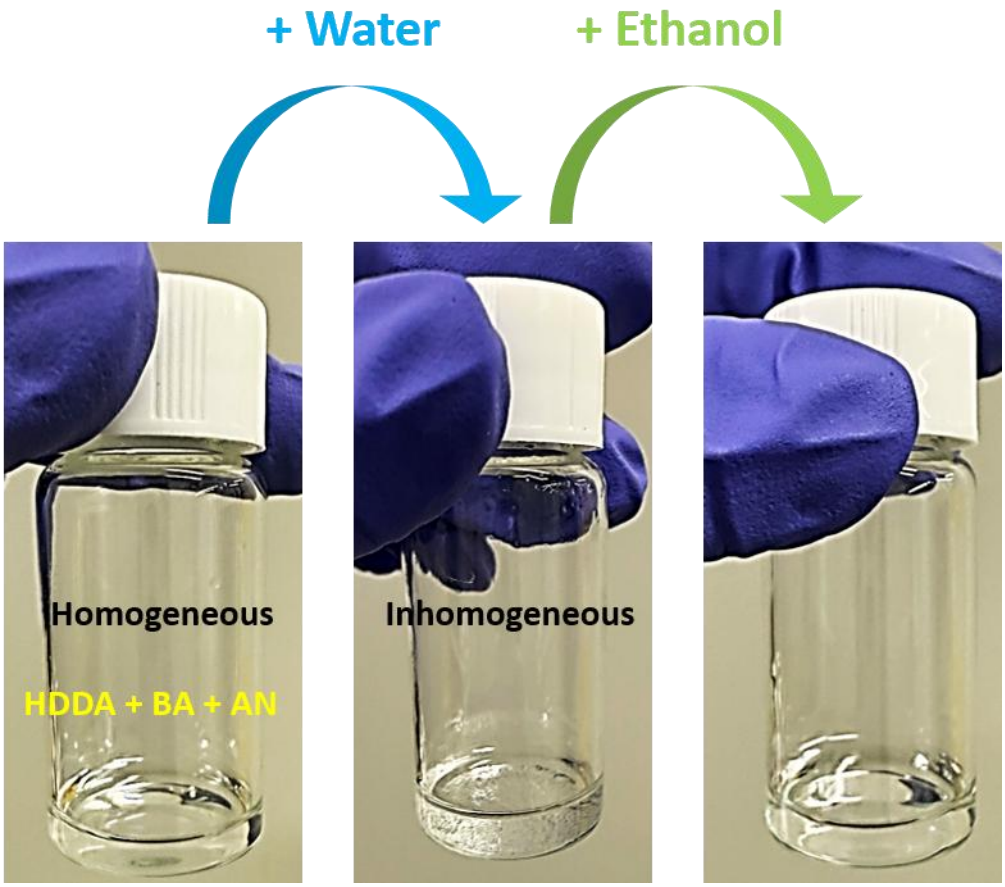

Fig. S1. Digital images showing inhomogeneous mixing induced by an antisolvent (water) and homogeneous mixing achieved with a cosolvent (ethanol).

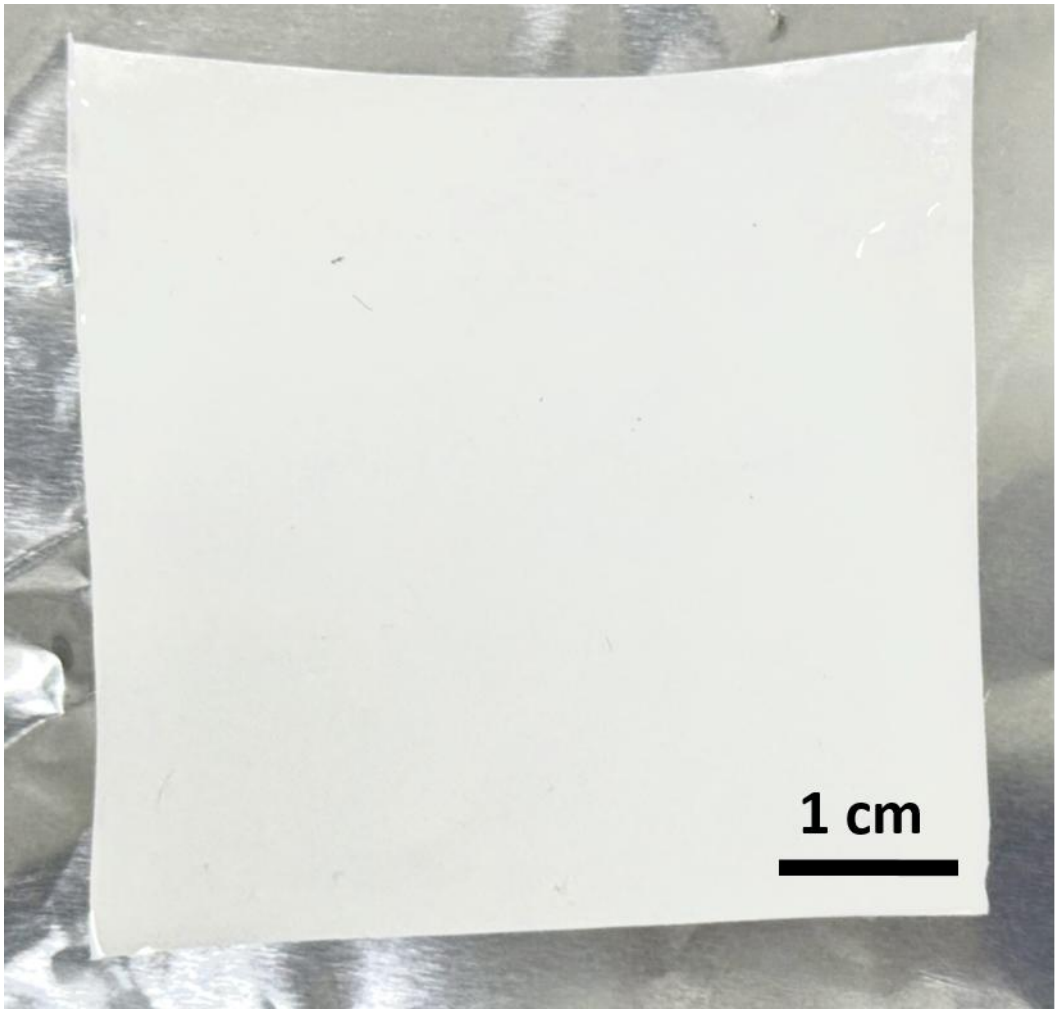

Fig. S2. Photograph of a scalable PHBA separator.

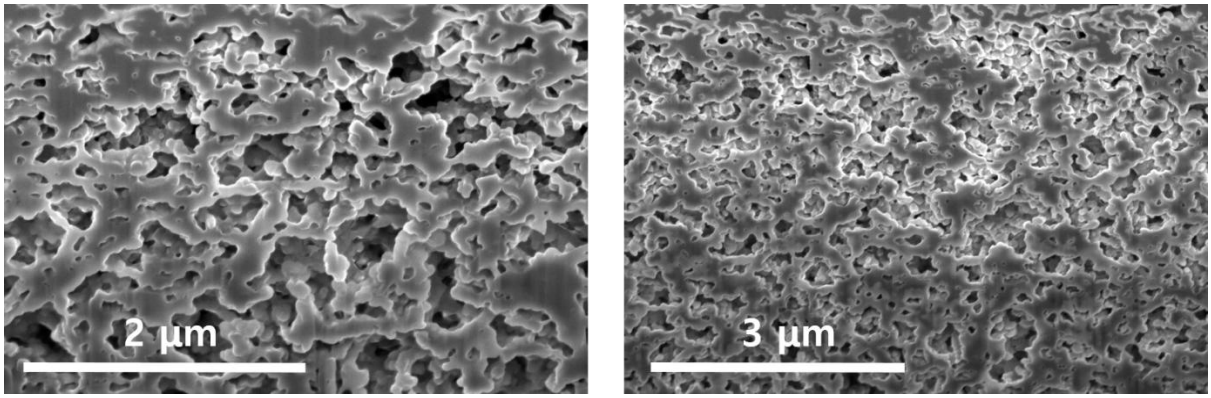

Fig. S3. FIB-SEM images of the PHBA separator at different magnifications.

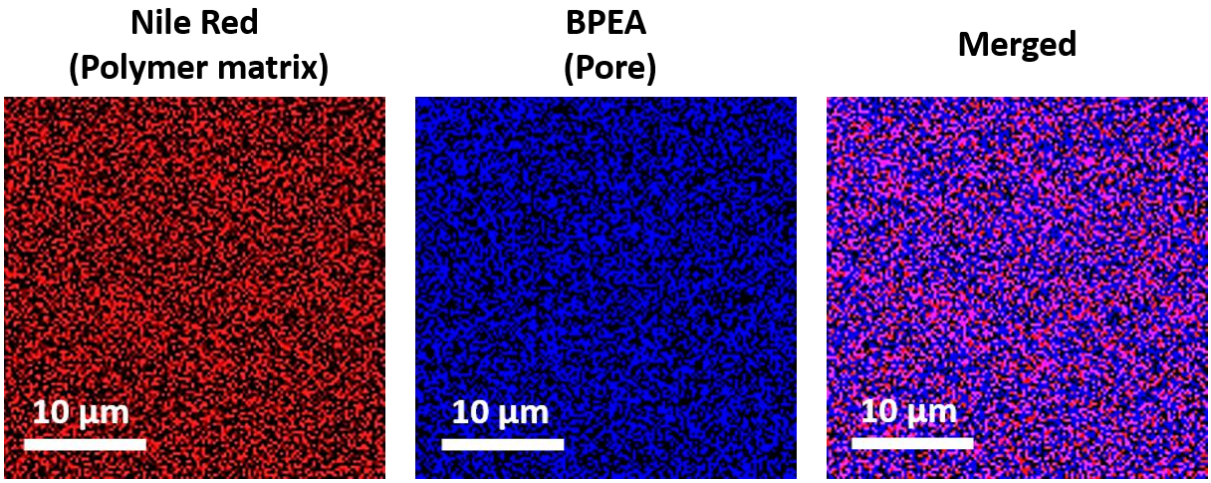

Fig. S4. Confocal laser scanning microscopy (CLSM) images of the porous PHBA separator: polymer matrix stained with Nile Red (red), pore regions stained with BPEA (blue), and merged image showing both polymer and pores.

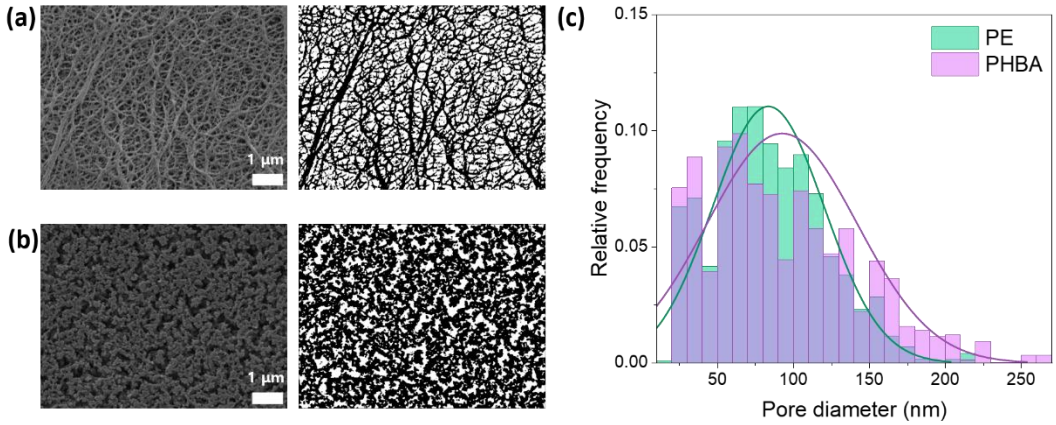

Fig. S5. (a) SEM image (left) and corresponding thresholded binary map (right) of the PE separator. (b) SEM image (left) and corresponding thresholded binary map (right) of the PHBA separator. (c) Overlaid pore size distributions extracted from the thresholded SEM images. The mean pore diameters were 83.6 ± 36.9 nm for PE and 92.6 ± 49.5 nm for PHBA.

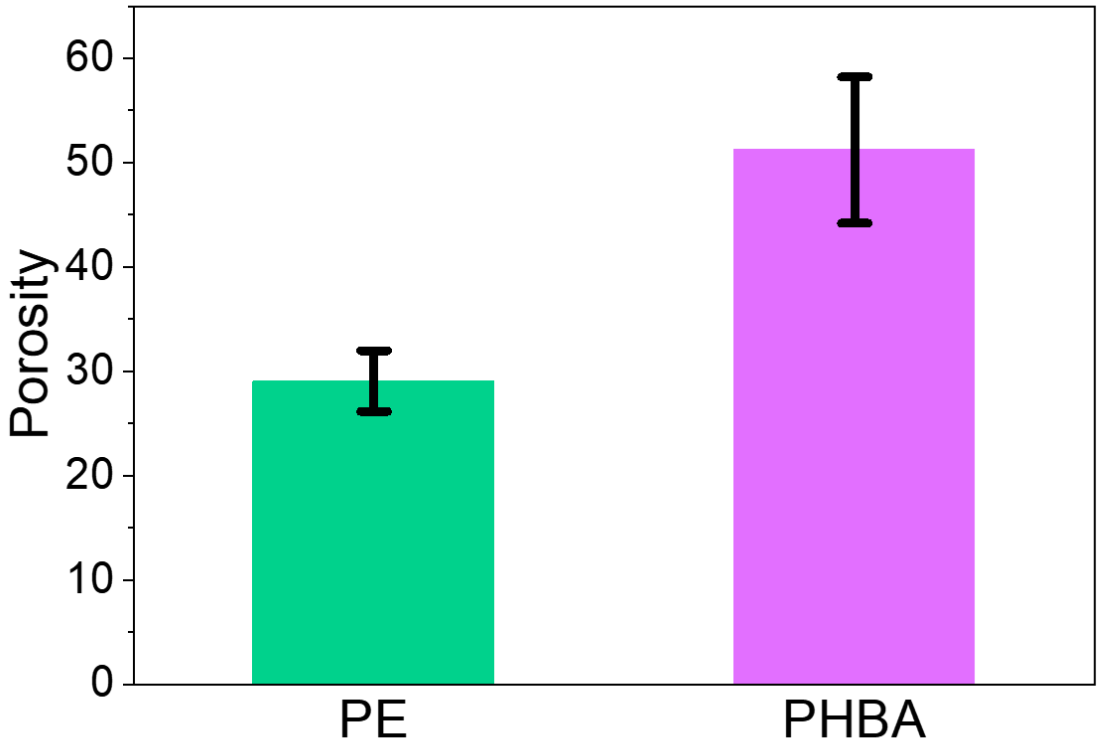

Fig. S6. Porosity of PE and PHBA separators measured by the *n*-butanol uptake test.

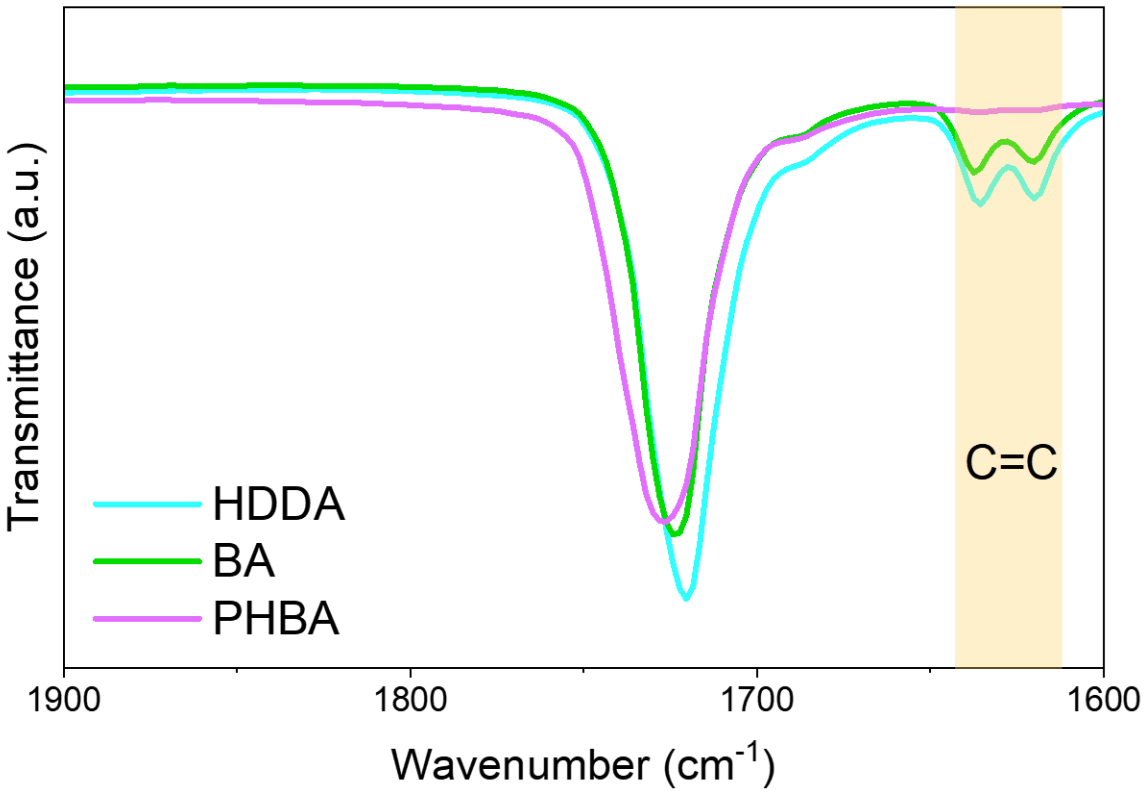

Fig. S7. FT-IR spectra of HDDA, BA, and the PHBA separator.

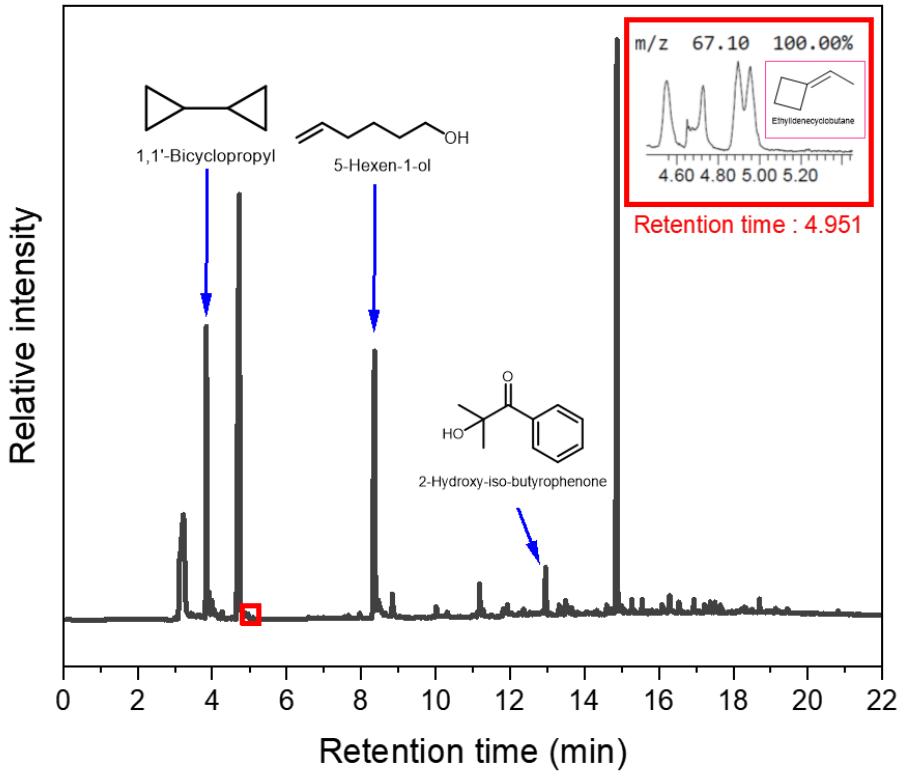

Fig. S8. Py-GC/MS spectra of the PHBA separator.

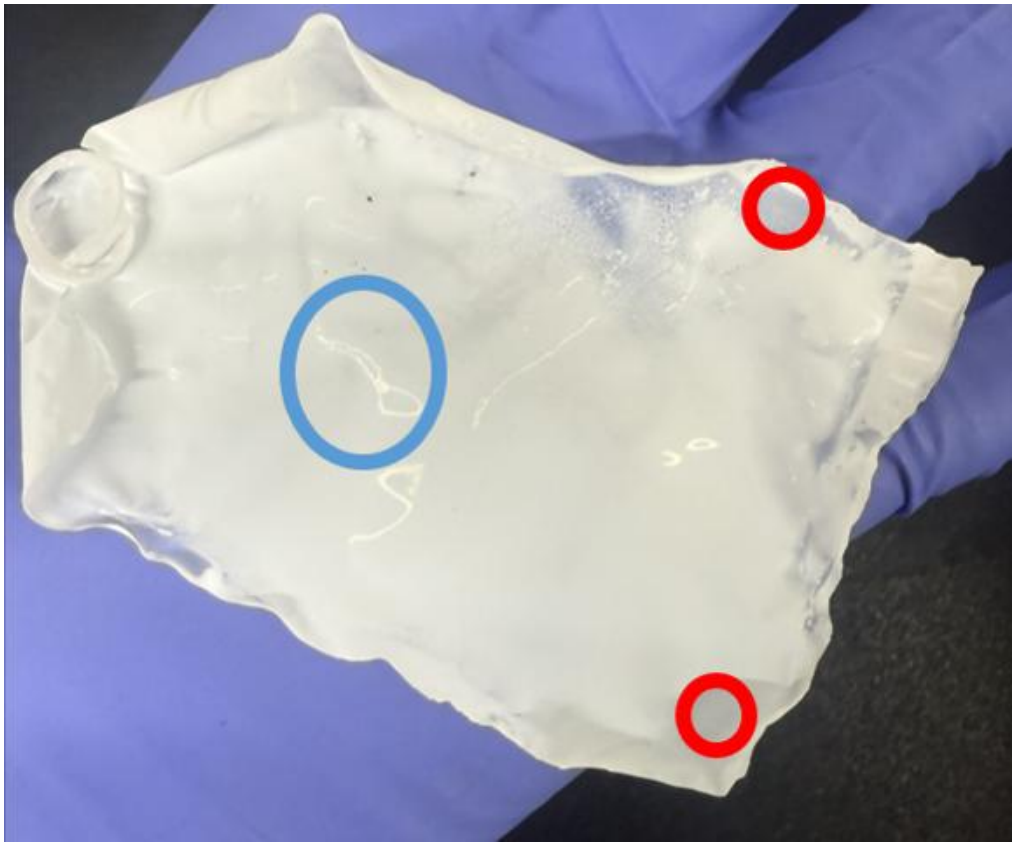

Fig. S9. Photograph of the PHBA separator with a monomer ratio of HDDA:BA = 2:3.

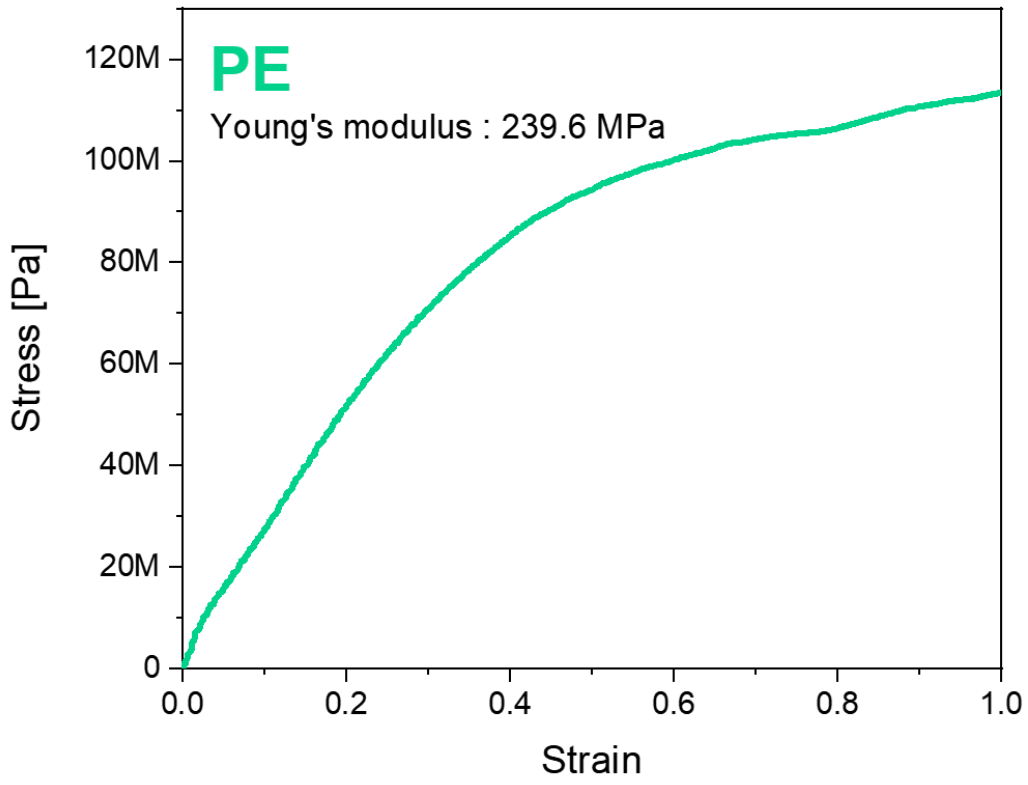

Fig. S10. Stress–strain curve of the PE separator.

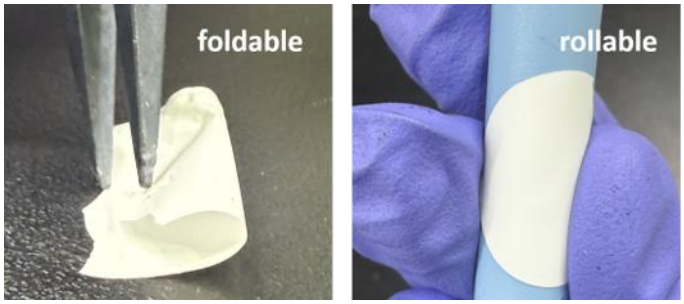

Fig. S11. Photographs of the foldable and rollable PHBA separator.

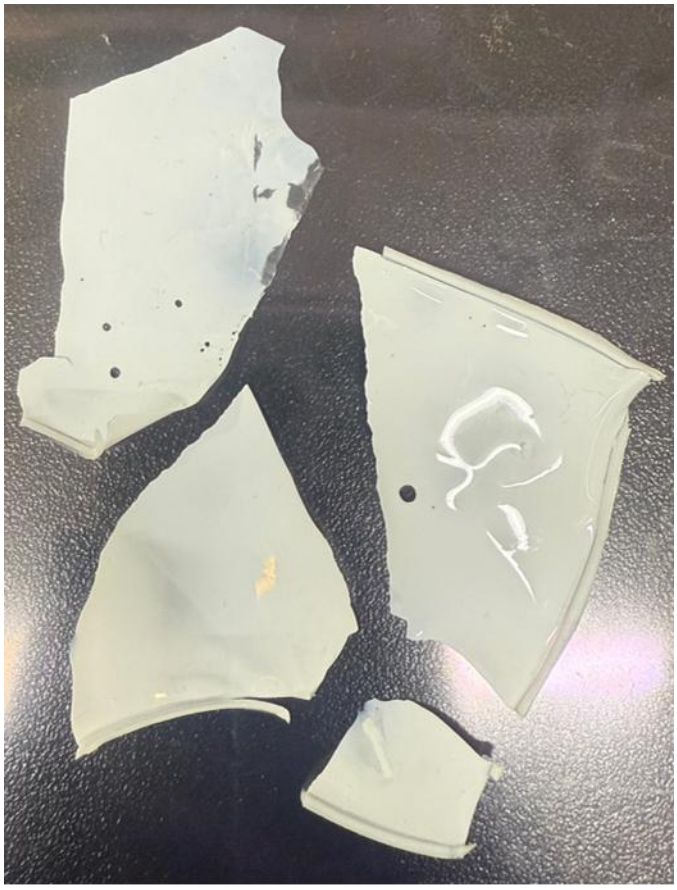

Fig. S12. Photograph of the PHBA separator with an AN ratio of 1.5.

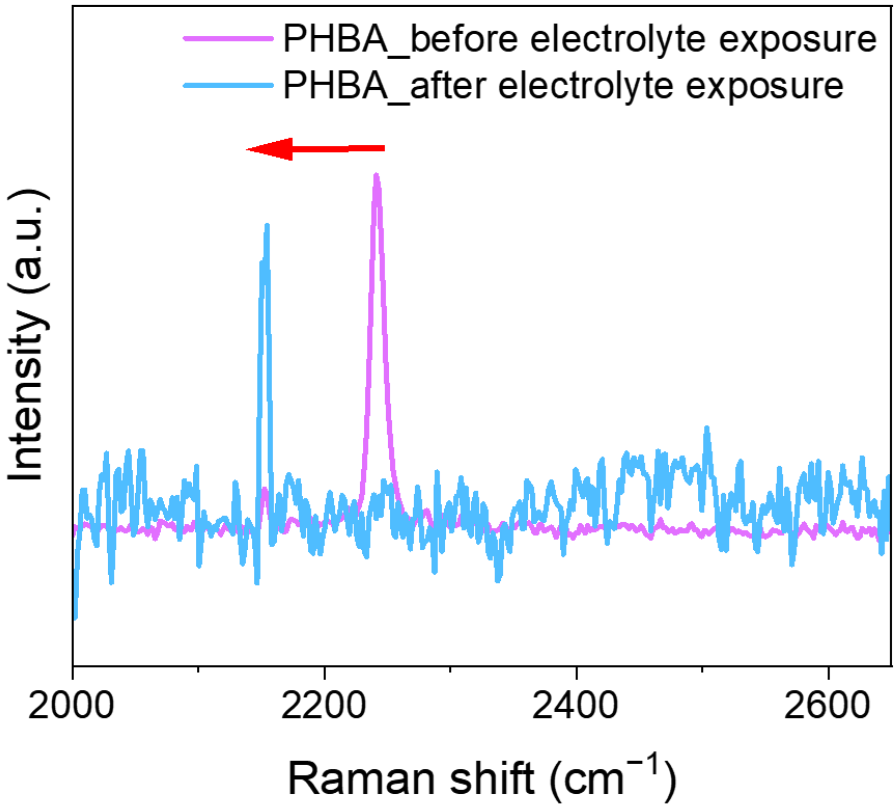

Fig. S13. Raman spectra of the PHBA separator before and after electrolyte exposure, showing a red-shift of the C≡N stretching band after exposure.

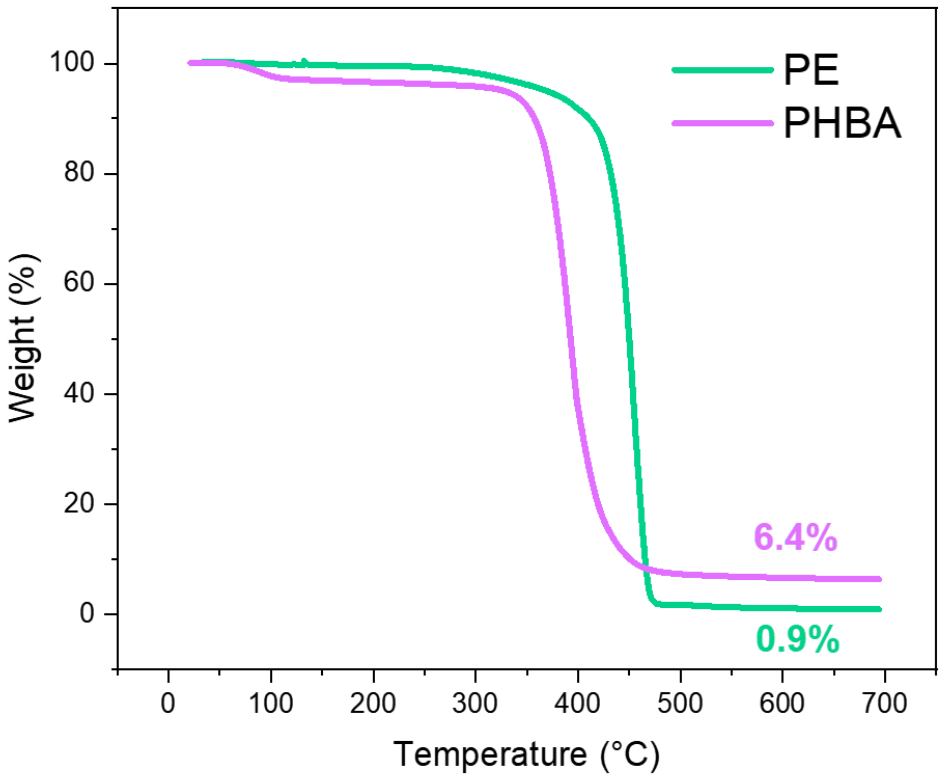

Fig. S14. TGA curves of PE and PHBA separators.

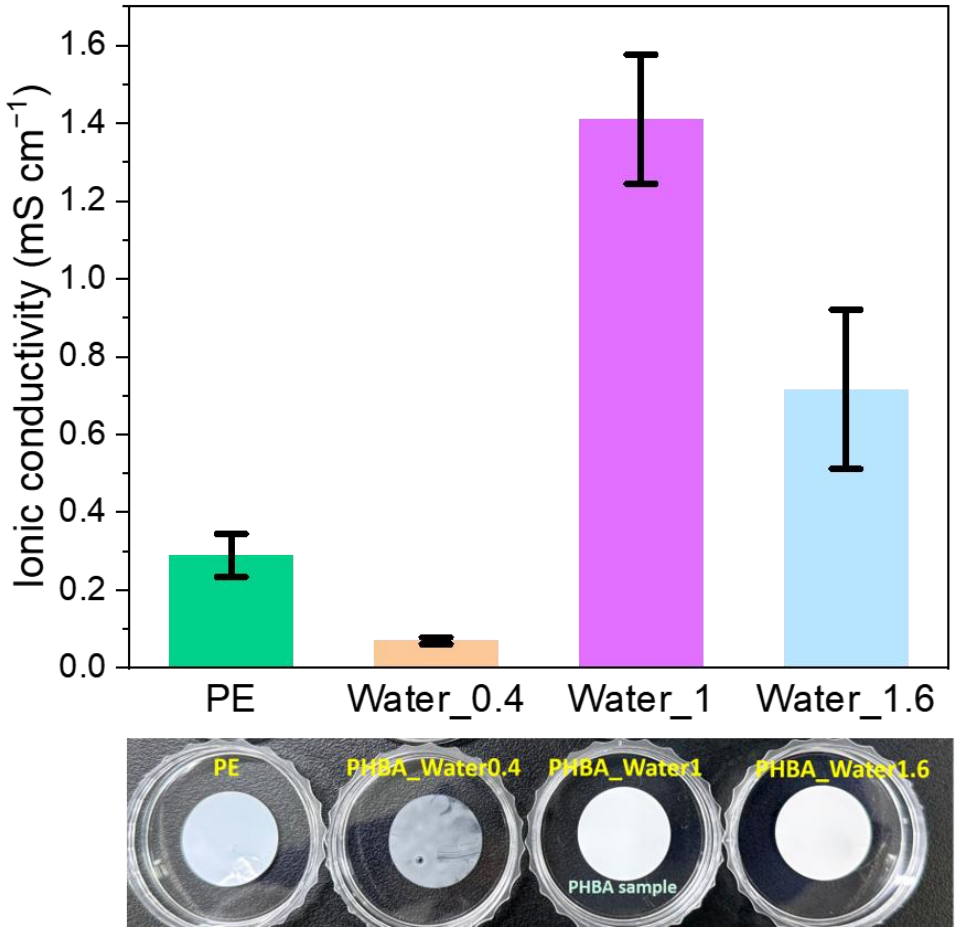

Fig. S15. Ionic conductivity of PE separator and PHBA separators prepared with different water contents.

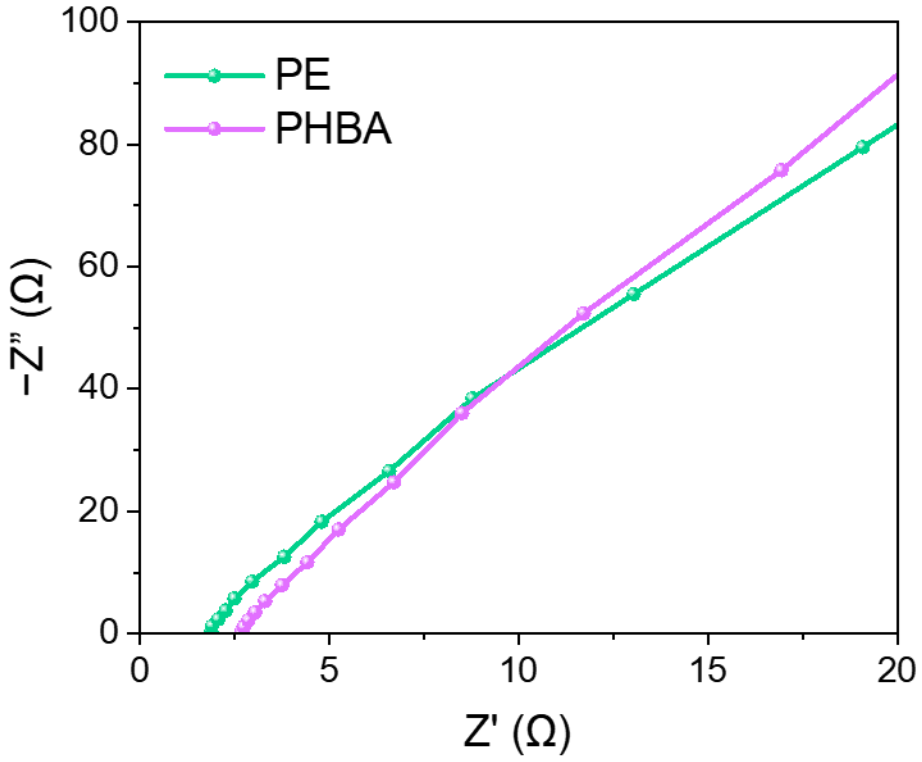

Fig. S16. Nyquist plots of SS/SS cells with PE and PHBA separators based on median ionic conductivity values.

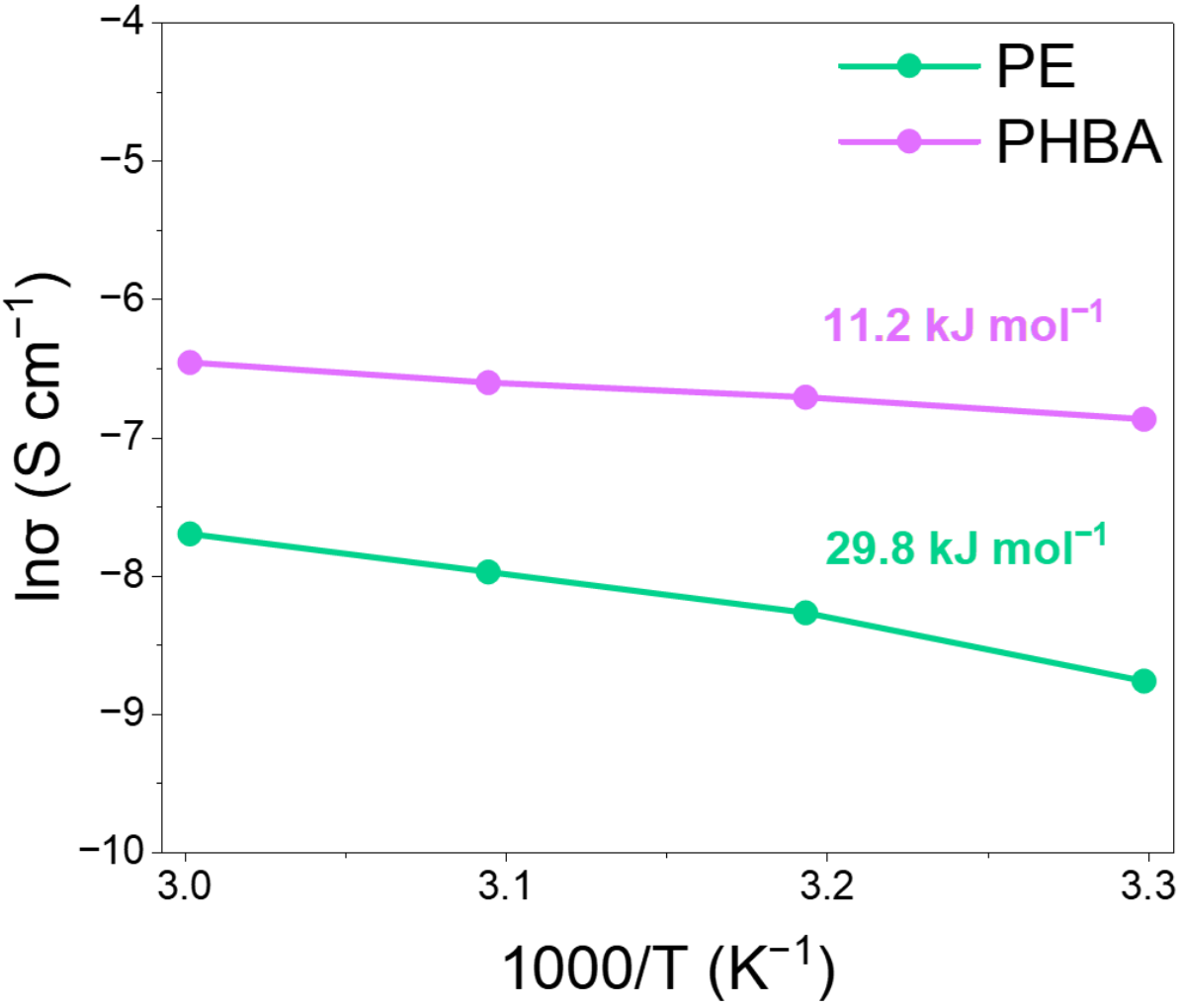

Fig. S17. Arrhenius plots of PE and PHBA separators used to extract activation energy (E_a).

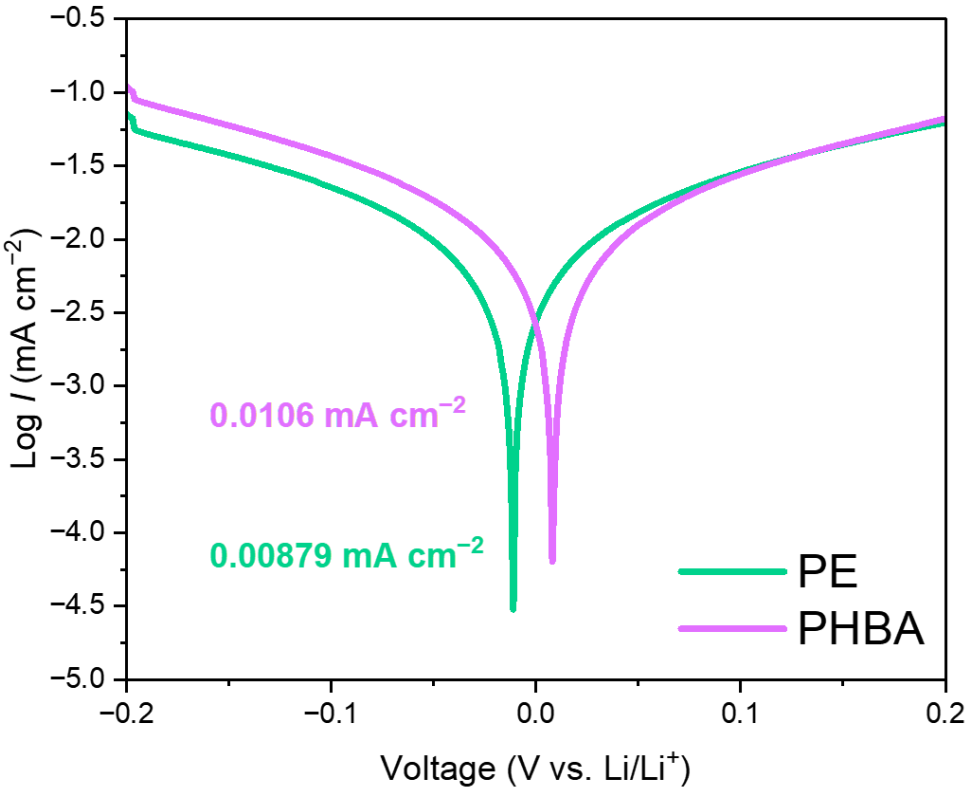

Fig. S18. Tafel plots of PE and PHBA separators.

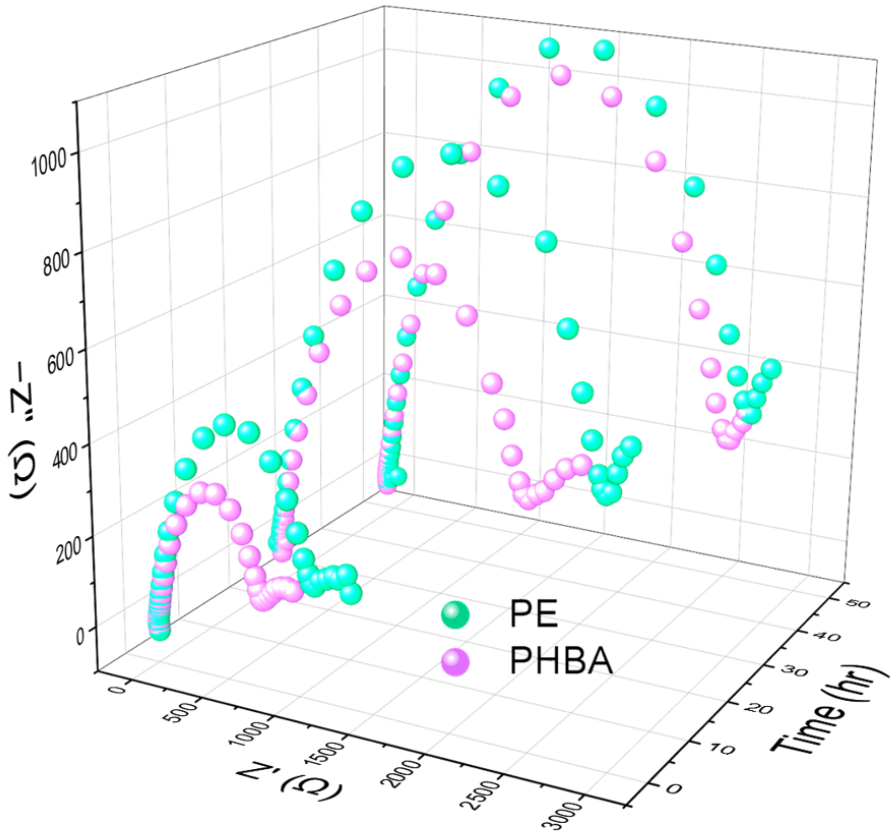

Fig. S19. Nyquist plots of PE and PHBA separators measured by EIS in symmetric Li/Li cells at 0, 24, and 48 hours.

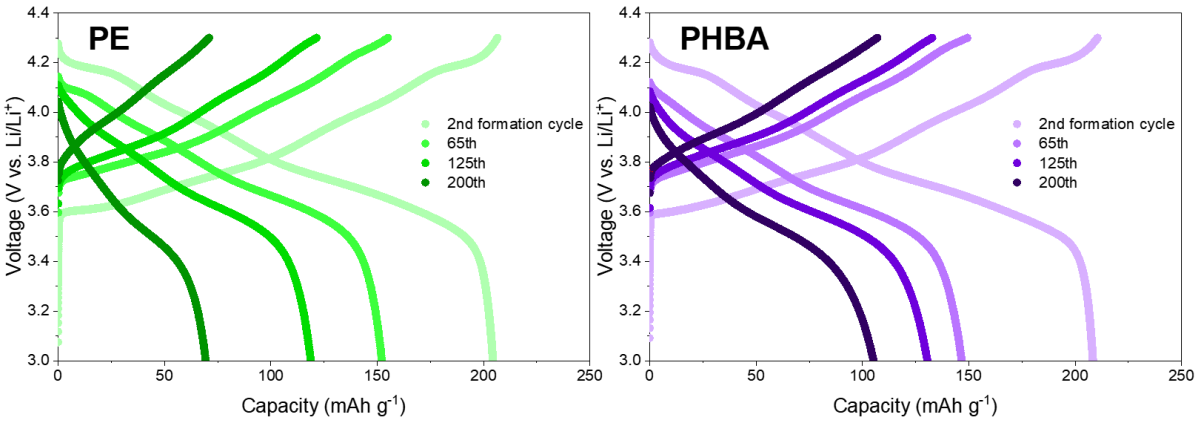

Fig. S20. Selected charge-discharge voltage profiles of Li/NCM811 full cells with PE and PHBA separators cycled at 2C and 30 ℃, shown for the 2nd cycle of the 0.1C formation step, the representative pre-crossover cycle (65th cycle), the representative post-crossover cycle (125th cycle), and the final cycle (200th cycle).

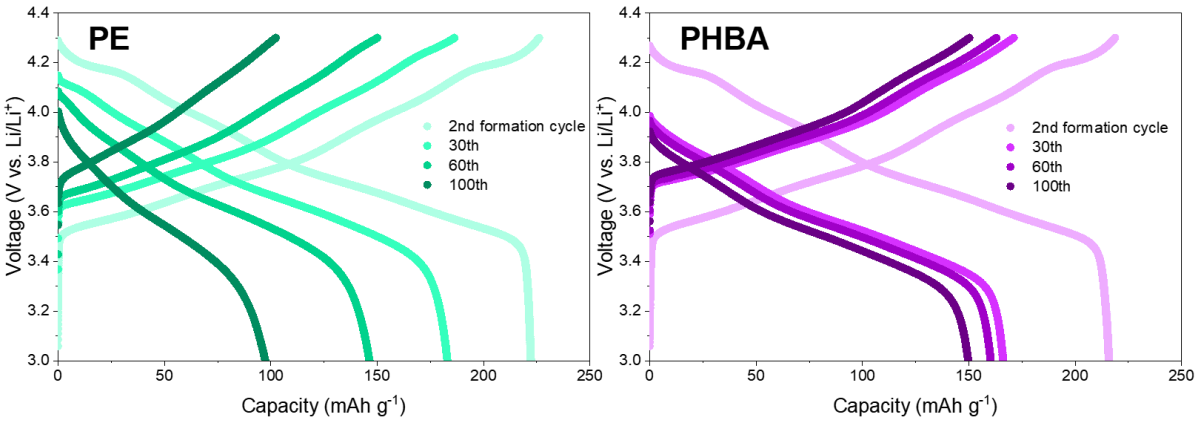

Fig. S21. Selected charge-discharge voltage profiles of Li/NCM811 full cells with PE and PHBA separators cycled at 1C and 60 ℃, shown for the 2nd cycle of the 0.1C formation step, the representative pre-crossover cycle (30th cycle), the representative post-crossover cycle (60th cycle), and the final cycle (100th cycle).

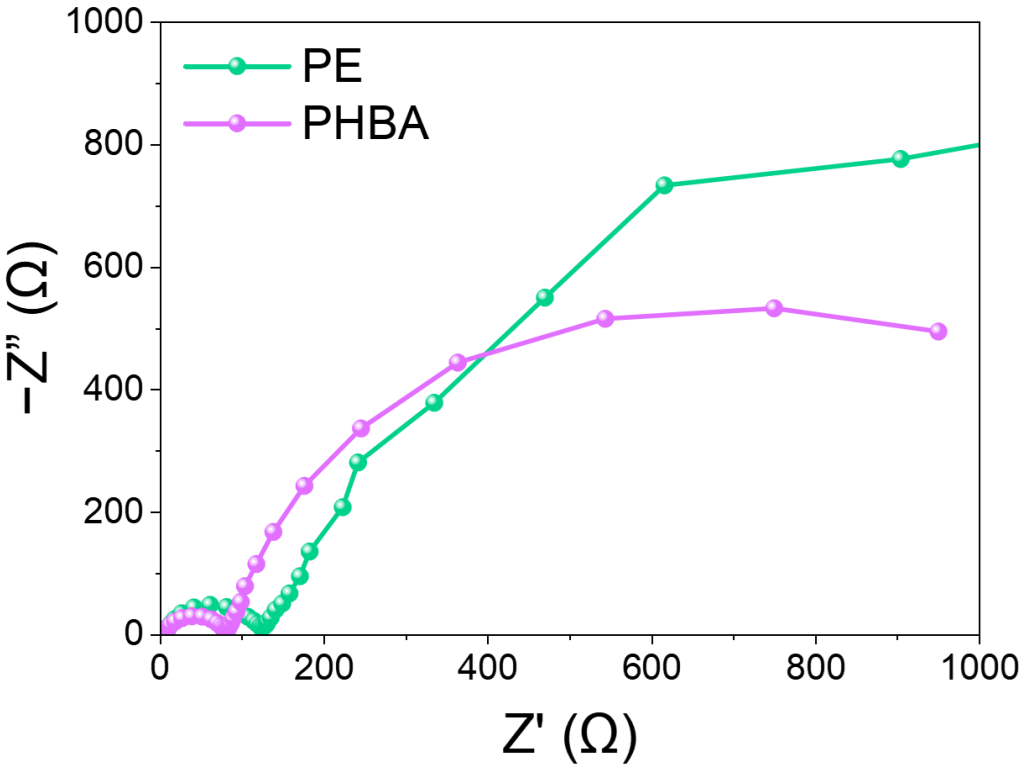

Fig. S22. Nyquist plots of EIS after 100 cycles at 1C and 60 ℃ within 3.0–4.3 V.

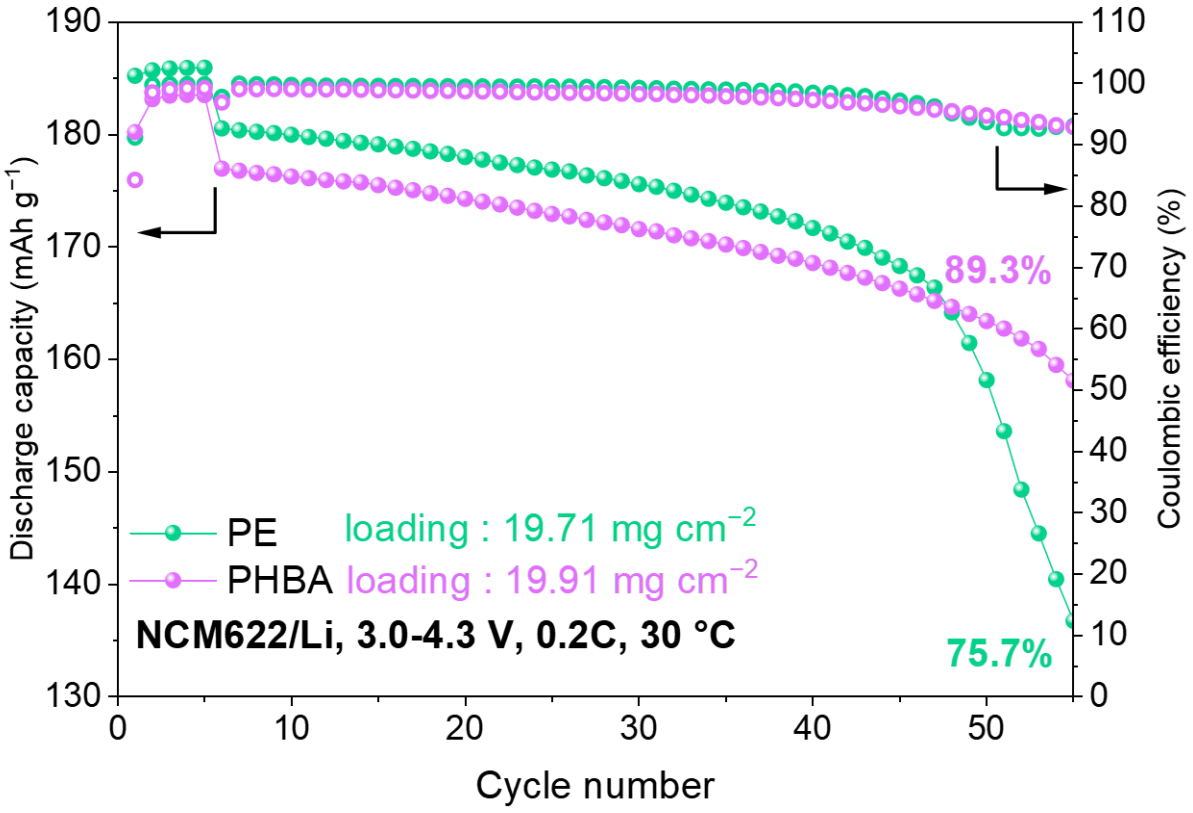

Fig. S23. Cycling performance of Li/NCM622 cells using PE or PHBA separators with high-areal-loading NCM622 cathodes (~20 mg cm^{-2}, ~100 μm). After five formation cycles at 0.1 C, cells were cycled at 0.2 C for 50 cycles at 30 ℃ within 3.0–4.3 V (1C = 177 mAh g^{-1}). Capacity retention was calculated by comparing the 55th cycle with the 6th cycle.

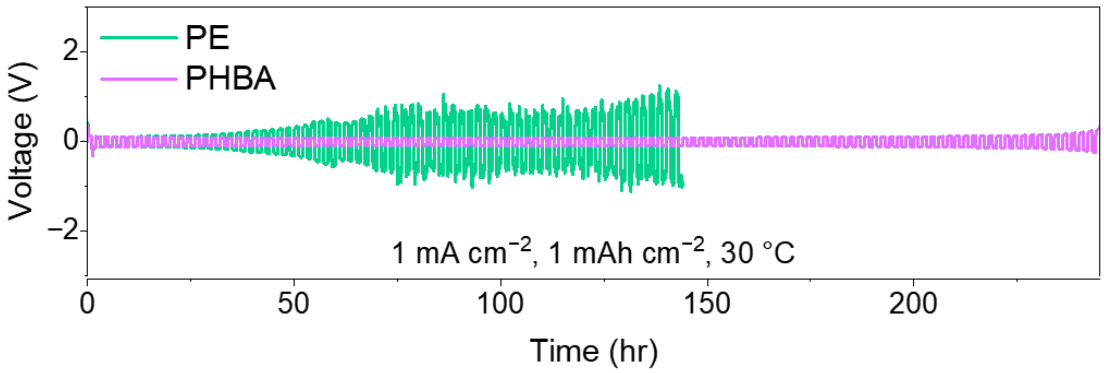

Fig. S24. Galvanostatic voltage profiles of Li/Li symmetric cells with PE and PHBA separators under 1 mA cm^{-2} with a capacity of 1 mAh cm^{-2}.

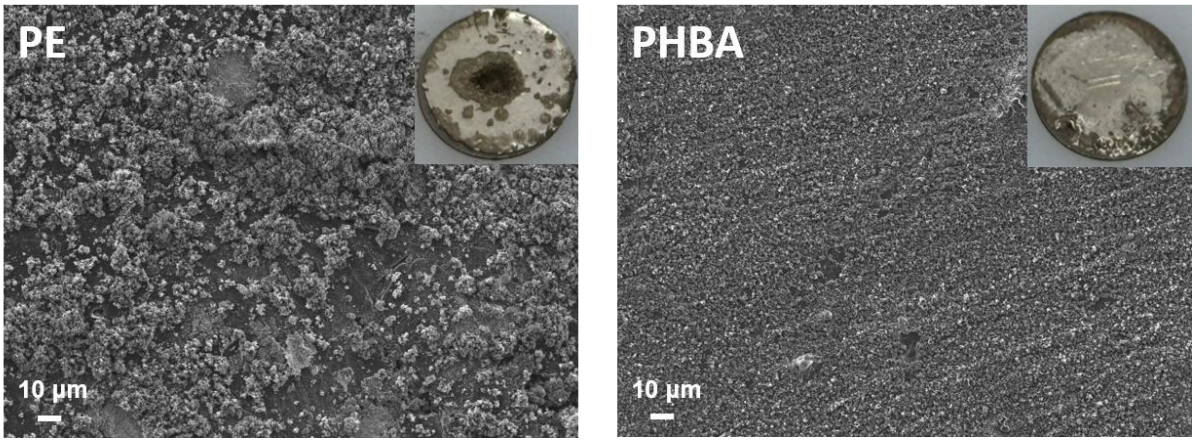

Fig. S25. SEM images of Li metal surfaces after cycling in Li/Li symmetric cells using PE and PHBA separators. Insets show the corresponding digital photographs of the Li metal surfaces.

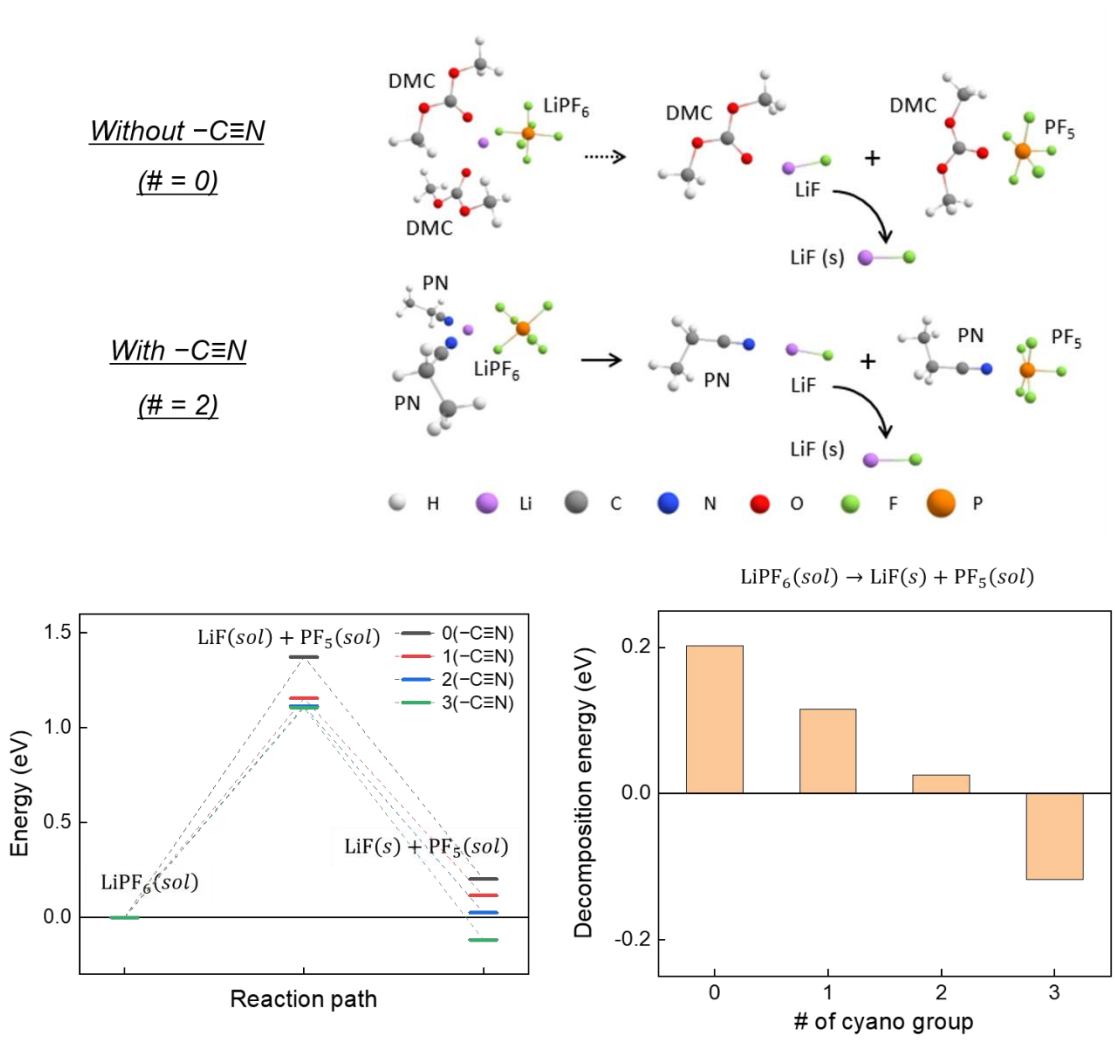

Fig. S26. DFT-derived reaction pathway and energetics for $LiPF_6$ decomposition toward LiF formation. Top: representative reaction schemes for models with 0 nitrile (C≡N) groups and 2 nitrile groups, following two sequential steps: $LiPF_6$(sol) → LiF(sol) + PF_5(sol) and LiF(sol) → LiF(s). Bottom left: reaction-path energy profiles for models containing 0–3 nitrile groups. Bottom right: overall decomposition energies for $LiPF_6$(sol) → LiF(s) + PF_5(sol) as a function of the number of nitrile groups.

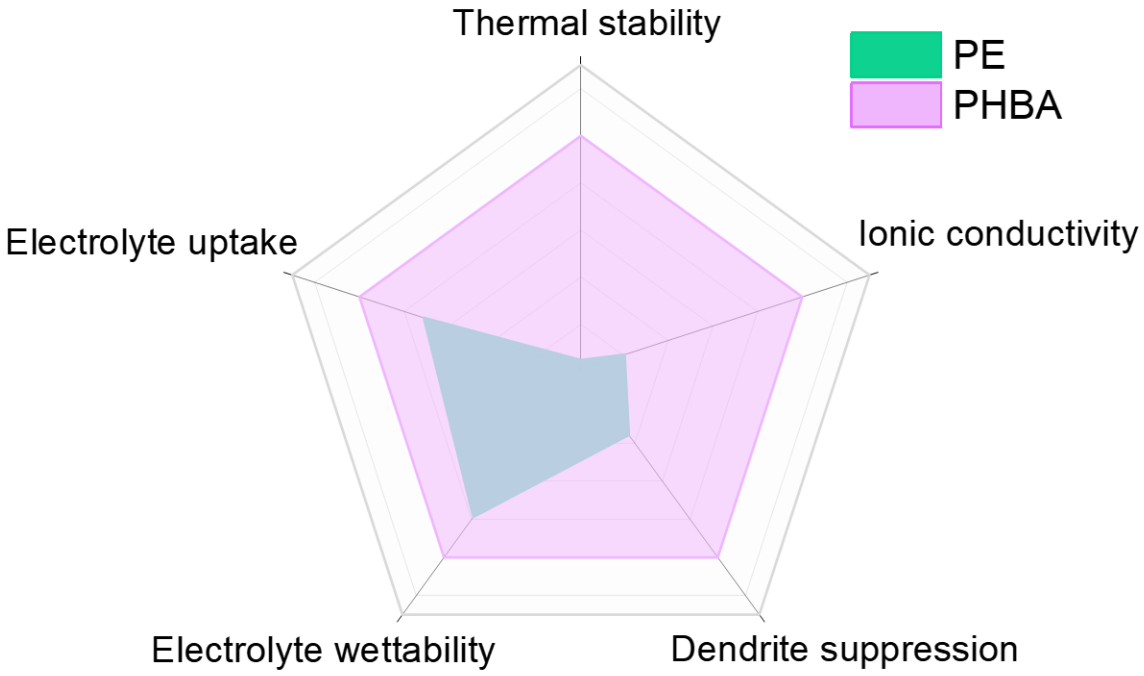

Fig. S27. Radar plot comparing key characteristics of PE and PHBA separators.

Table S1. Optimized ratios of monomers and solvents.

	HDDA	BA	AN	Water	EtOH	HMPP (Photoinitiator)
Vol. ratio	3	2	1	1	3.0±0.2	6 μL